Topological Boundary Time Crystal Oscillations

Dominik Nemeth,[*] Ahsan Nazir, Alessandro Principi, and Robert-Jan Slager

Department of Physics and Astronomy, The University of Manchester,
Oxford Road, Manchester M13 9PL, United Kingdom
(Dated: February 23, 2026)

Boundary time crystals (BTCs) break time-translation symmetry and exhibit long-lived, robust oscillations insensitive to initial conditions. We show that collective spin BTCs can admit emergent topological winding numbers in operator space. Expanding the density operator in a spherical tensor basis, we map the Lindblad dynamics onto an effective local hopping problem, where collective degrees of freedom label sites of an emergent two-dimensional operator space lattice and identify topological obstructions that enforce the delocalization of operator modes on the lattice. The resulting spectral delocalization provides a natural explanation for the robust oscillatory dynamics observed in BTCs. When combined with non-reciprocal transport of operator weight across operator space, this mechanism moreover also leads to the universality of long-time dynamics across a broad class of initial states. Our results frame BTC dynamics as a form of topologically constrained operator space transport and suggest a close connection to non-Hermitian skin-effects.

Introduction.—Time crystals have emerged as a central concept in nonequilibrium quantum physics, revealing new forms of dynamical order characterized by persistent oscillations in time [1–15]. Beyond their original formulation in closed and periodically driven systems, increasing attention has focused on time-crystal phases in open quantum systems, where dissipation and decoherence can play a constructive role in realizing long-lived oscillations [16–22].

A particularly striking realization is the boundary time crystal (BTC) [23], which arises in collective spin systems weakly-coupled to Markovian environments. In this model, oscillations persist indefinitely in the thermodynamic limit despite the presence of dissipation, making BTCs robust realizations of time-crystalline behavior in many-body systems. Recent developments have shown that BTCs can be understood in the basis of spherical tensor operators [24], where the dynamics is described in terms of operator space quantum numbers (as opposed to state-based labels). BTCs then naturally emerge as a case where these quantum numbers are not conserved.

On a seemingly distinct front, topological concepts have provided a powerful framework for understanding properties and responses of condensed matter systems by focusing on the global structure of eigenstates, rather than microscopic details. In terms of systems that admit an effective band description, a rather unified understanding has emerged [25–29] that has recently been related to the wider concept of quantum geometry [30, 31]. These geometric interpretations are increasingly being proven to be valuable in the study of various types of effective responses [32–35]. This topological lens has additionally also been the subject of active interest in non-Hermitian systems, that is systems described by an effective non-Hermitian Hamiltonian obtained by neglecting the Lindbladian quantum jump term [36–38]. Due to the non-Hermiticity and resulting complex energies, usual line-gap classifications can in such systems be extended by point-gap topologies, in which a winding number around a singular point is defined [39, 40]. Such point-gap topologies can have a striking consequence in terms of inducing a non-Hermitian skin effect [36, 41, 42], whereby a net drift across a chain forces the accumulation of eigenmodes at the boundary of this chain.

Recent work has demonstrated that key concepts of non-Hermitian topology, such as winding numbers and the skin effect, can be extended to Lindbladian superoperators [43–54]. In the class of quadratic Lindbladians, a direct relation can be established between the winding numbers of the Lindbladian and those of the associated postselected non-Hermitian Hamiltonian [54]. While these quadratic systems possess an intrinsic notion of spatial locality, an analogous concept can emerge in collective spin systems, where locality is instead realized in operator space [24].

In this Letter, we uncover that certain BTC dynamics can be understood in terms of *operator space topology*, providing a unified explanation for their robust oscillations and, crucially, their initial-state independence. Remarkably, collective spin BTCs admit an effective mapping to a non-Hermitian hopping problem in operator space, where collective degrees of freedom label sites of an emergent two-dimensional geometry [24]. In this setting, coherent and dissipative processes generate position-dependent hoppings, giving rise to a highly inhomogeneous transport landscape. We diagnose the local topology of this emergent space using the spectral localizer [55–57], viewed as a probe of operator space position. Using this probe, we identify local Chern-type markers and demonstrate how non-zero topological indices lead to the delocalization of eigenmodes in operator space. We demonstrate how this topology generically produces robust BTC oscillations. We finally showcase these results in simple model settings.

Model and Spherical Tensors.—BTCs arise in collective spin systems governed by a Markovian Lindblad mas-
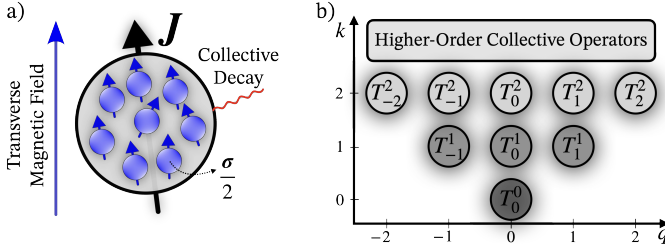
FIG. 1. Collective Spin System and Spherical Tensor Operators. a) Schematic diagram of the BTC model in Eq. (1), showing the collective spin configuration for the maximally polarized subsector $j = N/2$. b) Spherical tensor basis [Eq. (2)] shown as operator multiplets, where the kth multiplet contains $(2k + 1)$ operators. Here, $T_0^0 \propto \mathbb{I}$ and the triplet (T_{-1}^1, T_0^1, T_1^1) is equivalent to (J_-, J_z, J_+) up to normalization factors. The multiplets form a wedge-shaped lattice, whose sites are the spherical tensor operators.

ter equation, $\dot{\rho} = \mathcal{L}\rho$, where ρ is the density operator and $\mathcal{L}$ the Liouvillian superoperator. The canonical BTC model can be written as,

$$\dot{\rho} = -i[H, \rho] + \frac{\Gamma}{N}\Big(J_-\rho J_+ - \frac{1}{2}\{J_+J_-, \rho\}\Big), \quad (1)$$

where $H = \Omega J_x$ describes uniform coupling to a transverse field, while the dissipator produces collective decay with rate Γ [see Fig. 1a)]. The collective spin-j operators J_α ($\alpha = x, y, z$) are built from N underlying spin-$\frac{1}{2}$ degrees of freedom such that $j = N/2$. Finally, $J_\pm = J_x \pm iJ_y$. In the mean-field limit, this model exhibits a BTC phase for sufficiently strong coherent driving, $\Gamma/\Omega < 1$ [23], characterized by persistent oscillations. A natural basis is provided by the spherical tensor operators T_q^k [24],

$$\rho = \sum_{k=0}^{2j} \sum_{q=-k}^{+k} a_{kq} T_q^k, \quad (2)$$

where the spherical tensor rank k may take the values $k = 0, 1, ..., 2j$ and q is a magnetic quantum number with allowed values $q = -k, ..., +k$ [58, 59]. The tensor rank k provides a natural measure of operator complexity: low-rank tensors correspond to simple collective observables, such as the spin operators $J_{x,y,z}$ for $k = 1$, while higher-rank tensors encode increasingly complex collective correlations. Coupling between different k sectors therefore represents dynamical mixing between observables of different complexity. The magnetic index q labels internal levels within each fixed-k sector. For example, for $k = 1$, the spherical tensors (T_0^1, T_1^1, T_{-1}^1) are each related to the collective spin operators (J_z, J_+, J_-) respectively.

Mapping to the Non-Hermitian Hopping Model—Within this representation, the labels k and q can be interpreted as the coordinates of a two-dimensional wedge shaped lattice as shown in Fig. 1b). Importantly, the ac-

tion of the superoperator $\mathcal{L}$ can be reinterpreted as hoppings on this lattice. Dissipative processes can induce non-reciprocal hoppings between neighbouring k ranks and on-site decay, while coherent $(-i[H, \cdot])$ terms generate reciprocal hoppings between neighbouring q levels.

Expanding ρ in the basis $\{T_q^k\}$ [Eq. (2)] maps Eq. (1) to an effective 2D non-Hermitian hopping model [24],

$$\begin{aligned} \dot{a}_{k,q} = &t_+(k, q)\, a_{k+1,q} + t_-(k, q)\, a_{k-1,q} \\ &- \gamma(k, q)\, a_{k,q} - iw(k, q)\big(a_{k,q-1} + a_{k,q+1}\big), \quad (3) \end{aligned}$$

where a_{kq} is the corresponding operator weight of the spherical tensor with rank k and index q. Hopping along the effective coordinate k is described by $t_\pm(k, q) \propto \Gamma/N$, $\gamma(k, q) \propto \Gamma/N$ denotes on-site decay, while $w(k, q) \propto \Omega$ encodes hoppings along the coordinate q. The effective hopping amplitudes along the coordinate k are in general asymmetric, $t_+(k, q) \neq t_-(k, q)$, leading to the local, non-Hermitian hopping model interpretation. In this work, we will be focusing on the effective one-dimensional chain along the coordinate k, with the q levels compressed to an internal degree of freedom (in analogy with an SSH chain). For a spin-j collective spin model, the emergent chain has $(2j + 1)$ sites, with intrinsic open boundaries at $k = 0$ and $k = 2j$ as shown in Fig. 2a).

Topological Characterization.—We classify a local point-gap topology associated with the family of operators $x \mapsto \mathcal{L}(x) - \lambda_0$, where x labels the emergent coordinate on the operator chain and $\lambda_0 \in \mathbb{C}$ is a reference complex frequency. In a locally uniform region U, where the Liouvillian varies slowly in x, the system admits an approximate translation symmetry. One may then introduce a conjugate momentum $p \in S^1$ via a local Fourier transform. As p is varied around the circle, the map $p \mapsto \mathcal{L}_U(p) - \lambda_0$ defines a closed loop in the space of invertible operators. The winding of this loop provides the local topological invariant. If the map can be continuously deformed to a single point, then it is topologically trivial. If such a deformation is obstructed, the map necessarily exhibits a non-trivial winding, indicating a non-trivial *local point-gap topology* (see Fig. 2b)). The local point-gap topology and its corresponding non-trivial winding can be diagnosed via the spectral localizer framework [57]. This framework converts the initial problem into a Hermitian gap analysis, such that non-trivial windings are encoded into local topological indices.

The spectral localizer provides a position-space diagnostic of topology by asking whether a system can be locally and continuously deformed to an "atomic limit" while preserving both the relevant symmetries and a spectral gap [57]. In this atomic limit, the fundamental degrees of freedom are fully decoupled and behave as isolated constituents. Such a deformation implies the existence of a complete, localized Wannier basis and therefore places the system in a topologically trivial class.
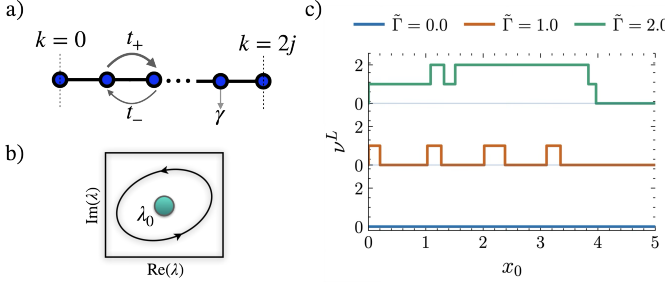
FIG. 2. Non-Hermitian Hopping Model and One-Dimensional Spectral Localizer Probe. a) Effective one-dimensional hopping chain along the probe coordinate k, constructed in the spherical tensor basis [Eq. (3)]. b) As p is varied along S^1, the map $p \mapsto \mathcal{L}_U(p) - \lambda_0$ traces a non-contractible loop in the complex plane, signaling a non-trivial winding around the point-gap at λ_0. c) Local topological index ν^L as a function of the sweep coordinate x_0, probing the rank chain shown in a). Results are shown for fixed $\lambda_0 = 0$ and $\tilde{\Gamma} \equiv \Gamma/\Omega = 0$, 1.0, 2.0 with $N = 20$ spins. Data are truncated to $x_0 \leq 5$ for clarity; ν^L remains zero beyond this range.

Conversely, when no such local deformation exists, the obstruction signals non-trivial topology—in the present context, a non-trivial point-gap winding of the spectrum. The spectral localizer formulates this obstruction directly in a position-resolved manner, enabling a local probe of topology even in systems without translational invariance.

For collective spin systems, a natural position-space description emerges from the effective local hopping model introduced in Eq.(3). In the following, we analyze the resulting one-dimensional chain shown in Fig. 2a). Accordingly, we introduce a position superoperator $\mathcal{X}$ as the projector onto k [24], whose eigenvalues correspond to the site labels $k = 0, 1, \ldots, 2j$. To probe the local topology, we define the spectral localizer at coordinate x_0 and complex frequency λ_0 as

$$
\begin{aligned}
L_{(x_0,\lambda_0)}(\mathcal{L}, \mathcal{X}) =& \mathrm{Re}(\mathcal{L} - \lambda_0 \mathbb{I}) \otimes \sigma_x + \mathrm{Im}(\mathcal{L} - \lambda_0 \mathbb{I}) \otimes \sigma_y \\
& + \kappa(\mathcal{X} - x_0 \mathbb{I}) \otimes \sigma_z,
\end{aligned}
\tag{4}
$$

where κ controls the relative strength of spatial and spectral terms, and the Pauli matrices $\sigma_{x,y,z}$ enforce an orthogonal embedding of spectral and positional directions [57]. By construction, the Hermitian operator $L_{(x_0,\lambda_0)}$ belongs to symmetry class AIII (see End Matter).

This construction converts the non-trivial point-gap winding into an integer-valued local topological invariant,

$$
\nu^L_{(x_0,\lambda_0)} = \frac{1}{2} \mathrm{sig}\Big[L_{(x_0,\lambda_0)}\Big],
\tag{5}
$$

where the signature is defined as the difference between the number of positive and negative eigenvalues. The

corresponding localizer gap is

$$
\mu_{(x_0,\lambda_0)} = \min\Big\{ |\lambda| : \lambda \in \mathrm{spec}\big(L_{(x_0,\lambda_0)}\big)\Big\},
\tag{6}
$$

where $\mathrm{spec}(L_{(x_0,\lambda_0)})$ denotes the spectrum of the (Hermitian) localizer evaluated at coordinate x_0 and complex reference frequency λ_0. The index ν^L is stable under any continuous deformation that preserves $\mu_{(x_0,\lambda_0)} > 0$; it can change only when the localizer gap closes, i.e., when an eigenvalue of $L_{(x_0,\lambda_0)}$ crosses zero, signalling a topological transition [57].

A non-zero value of $\nu^L_{(x_0,\lambda_0)}$ implies that $\mathcal{L}$ and $\mathcal{X}$ cannot be smoothly deformed to a mutually commuting, locally trivial limit without closing the gap $\mu_{(x_0,\lambda_0)}$ [57]. Consequently, there exists a topological obstruction to constructing operator modes that are simultaneously localized near position x_0 and sharply defined at complex frequency λ_0. Physically, this constitutes a no-go statement: the dynamics near (x_0, λ_0) cannot be reduced to independent, localized operator modes. In terms of the spherical tensor representation, this distinction has a clear interpretation. When $\nu^L_{(x_0,\lambda_0)} = 0$, Liouvillian eigenmodes can be constructed whose expansion coefficients a_{kq} are sharply peaked around a single tensor rank k_0, corresponding to localized operator modes in operator space. By contrast, when $\nu^L_{(x_0,\lambda_0)} \neq 0$, such localization is forbidden: any eigenmode with complex frequency near λ_0 must necessarily acquire support over an extended range of tensor ranks. The localizer index therefore diagnoses a fundamental incompatibility between localization in operator space and localization in complex frequency, enforcing delocalization of Liouvillian modes across spherical tensor sectors.

Signatures.—Fixing λ_0 to the steady-state eigenvalue and scanning the localizer along the operator space coordinate $x = k$, we observe the formation of position-dependent topological domains as the dissipation strength Γ increases, Fig. 2c). The index becomes non-zero only in specific rank sectors, indicating that the point-gap topology varies locally along the effective operator space chain.

The appearance of these domains coincides with the onset of delocalization of eigenmodes in operator space (see Fig. 4 in End Matter). In the topological regions, the steady-state eigenmode cannot be confined to a single tensor rank but instead spreads across multiple spherical-tensor sectors. Equivalently, operator weight is transported between different tensor ranks, which may be interpreted as local drifts in the effective hopping model that generate a net operator space transport within these regions.

Rather than fixing a complex frequency and probing the operator space chain, we may adopt the complementary perspective of fixing an operator space coordinate and resolving the entire complex frequency plane, see Fig. 3. This allows us to determine which Liouvillian
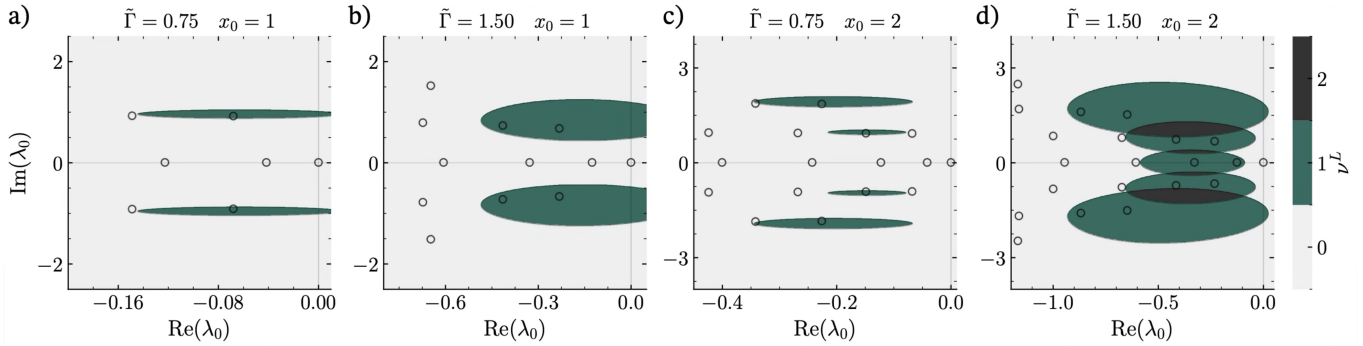
FIG. 3. Local Topological Islands. For fixed operator space coordinate x_0, we show the complex-frequency–resolved local index $\nu^L(\lambda_0)$ for four representative cases. Panels (a,b) correspond to $x_0 = 1$ with $\tilde{\Gamma} \equiv \Gamma/N = 0.75$ and 1.50, respectively, for $N = 10$. Panels (c,d) show the same parameter sets evaluated at $x_0 = 2$. Hollow circular markers denote the eigenvalues of the Liouvillian $\mathcal{L}$. Colour shading indicates the local value of ν^L, revealing spatially resolved regions of non-trivial topology in the complex-frequency plane.

eigenmodes are topologically robust when probing a specific set of operators.

Performing this spectral sweep reveals the emergence of isolated regions in the complex λ-plane where the localizer index is non-zero, forming topological "islands" in spectral space. These islands act as *local Chern-type markers* in spectral space: they signal a topological obstruction associated with modes at those complex frequencies when projected onto the chosen operator sector.

Crucially, we find that these topological islands host the slowest-decaying oscillatory modes of the Liouvillian spectrum, Figs. 3a) and 3b). These modes dominate the long-time dynamics and are responsible for the persistent oscillations characteristic of the BTC phase [23]. Since they necessarily carry a non-zero ν^L, they constitute *topological oscillatory modes*: their existence and spectral isolation are protected against local, continuous deformations of $\mathcal{L}$. This provides a natural explanation for the robustness of BTCs, directly linking their long-lived oscillatory behavior to an underlying, observable-resolved operator space topology.

The localizer framework naturally extends beyond simple collective spin observables to higher-order tensor rank sectors, which correspond to measurements of genuine many-body correlations not fully captured by mean-field descriptions restricted to $k = 1$ [60–62].

Focusing on the $k = 2$ sector, we observe an increase in the number of islands in the complex-frequency plane, Fig. 3c). These islands host additional slow-decaying oscillatory modes, indicating that higher-order observables support an even richer set of topologically protected dynamical modes.

As the dissipation strength is increased, these spectral islands expand and eventually merge, Fig. 3d). Physically, this reflects the fact that stronger dissipation enhances the coupling between different operator space sectors, causing topological obstructions associated with distinct modes to overlap. Consequently, robust oscillatory dynamics is not confined to mean-field observables, but is strengthened in higher-order many-body operator sectors.

Most importantly, this behavior is universal across a broad class of initial states. This universality can be directly traced to the delocalization of Liouvillian eigenmodes in operator space, which gives rise to an effective transport of operator weight between different tensor-rank sectors. As a result, even if an initial state is localized around an arbitrary position in operator space, its operator weight is not confined there but can flow across tensor ranks and into topological regions that support long-lived oscillatory modes.

This picture is further reinforced by the effective non-Hermitian hopping model itself [Eq. (3)], which permits transitions both along k and q. Consequently, operator weight generically explores operator space and is naturally funneled into those modes responsible for robust oscillatory dynamics. This mechanism provides a natural explanation for the initial-state independence characteristic of BTCs.

Conclusions and Discussions.—By expressing collective spin dynamics in the natural spherical tensor basis, we have mapped the canonical BTC model [Eq.(1)] onto an effective non-Hermitian hopping problem in operator space [Eq.(3)]. Within this framework, we demonstrated that the underlying local point-gap topology can be diagnosed using the spectral localizer, giving rise to local Chern-type markers in spectral space. These topological obstructions provide a natural explanation for the robust oscillations observed in collective spin BTCs. Crucially, the non-trivial point-gap winding enforces delocalization of Liouvillian modes across operator space, and the resulting non-reciprocal transport of operator weight leads to universal long-time dynamical behavior across a broad class of initial states.

We further showed that these topological features are not restricted to a single observable sector. In particu-

lar, they are present both in the steady-state eigenmode and in higher-order collective operators, whose dynamics generically exhibits even richer oscillatory behavior due to the presence of multiple topologically protected, slow-decaying modes. These effects can be experimentally probed in systems such as molecular or nuclear spin gases [63], where spatial degrees of freedom are negligible and spin dynamics is inherently collective.

Looking ahead, our results motivate the exploration of operator space models that support genuinely higher-dimensional topological structures. While the BTCs studied here are most naturally understood as effective one-dimensional chains labeled by tensor rank k, with motion in the magnetic quantum number q occurring locally at each site, our findings suggest the possibility of realizing local Chern markers in the full (k, q) operator space geometry. Such behavior is expected to arise in models where these coordinates cannot be treated independently, opening new avenues for topological classification and control of many-body open quantum dynamics.

---

* dominik.nemeth@manchester.ac.uk

[1] F. Wilczek, Quantum Time Crystals, Phys. Rev. Lett. **109**, 160401 (2012).

[2] P. Bruno, Impossibility of Spontaneously Rotating Time Crystals: A No-Go Theorem, Phys. Rev. Lett. **111**, 070402 (2013).

[3] H. Watanabe and M. Oshikawa, Absence of Quantum Time Crystals, Phys. Rev. Lett. **114**, 251603 (2015).

[4] V. Khemani, A. Lazarides, R. Moessner, and S. L. Sondhi, Phase Structure of Driven Quantum Systems, Phys. Rev. Lett. **116**, 250401 (2016).

[5] V. Khemani, R. Moessner, and S. L. Sondhi, A Brief History of Time Crystals (2019), arXiv:1910.10745 [cond-mat.str-el].

[6] K. Sacha, Modeling spontaneous breaking of time-translation symmetry, Phys. Rev. A **91**, 033617 (2015).

[7] K. Sacha and J. Zakrzewski, Time crystals: a review, Reports on Progress in Physics **81**, 016401 (2017).

[8] D. V. Else, B. Bauer, and C. Nayak, Floquet Time Crystals, Phys. Rev. Lett. **117**, 090402 (2016).

[9] D. V. Else, B. Bauer, and C. Nayak, Prethermal Phases of Matter Protected by Time-Translation Symmetry, Phys. Rev. X **7**, 011026 (2017).

[10] D. V. Else, C. Monroe, C. Nayak, and N. Y. Yao, Discrete Time Crystals, Annual Review of Condensed Matter Physics **11**, 467 (2020).

[11] C. W. von Keyserlingk, V. Khemani, and S. L. Sondhi, Absolute stability and spatiotemporal long-range order in Floquet systems, Phys. Rev. B **94**, 085112 (2016).

[12] N. Y. Yao, A. C. Potter, I.-D. Potirniche, and A. Vishwanath, Discrete Time Crystals: Rigidity, Criticality, and Realizations, Phys. Rev. Lett. **118**, 030401 (2017).

[13] A. Lazarides and R. Moessner, Fate of a discrete time crystal in an open system, Phys. Rev. B **95**, 195135 (2017).

[14] M. P. Zaletel, M. Lukin, C. Monroe, C. Nayak, F. Wilczek, and N. Y. Yao, Colloquium: Quantum and classical discrete time crystals, Rev. Mod. Phys. **95**, 031001 (2023).

[15] J. Zhang, P. W. Hess, A. Kyprianidis, P. Becker, A. Lee, J. Smith, G. Pagano, I. D. Potirniche, A. C. Potter, A. Vishwanath, N. Y. Yao, and C. Monroe, Observation of a discrete time crystal, Nature **543**, 217 (2017).

[16] K. Seibold, R. Rota, and V. Savona, Dissipative time crystal in an asymmetric nonlinear photonic dimer, Phys. Rev. A **101**, 033839 (2020).

[17] C. Lledó and M. H. Szymańska, A dissipative time crystal with or without Z2 symmetry breaking, New Journal of Physics **22**, 075002 (2020).

[18] C. Booker, B. Buča, and D. Jaksch, Non-stationarity and dissipative time crystals: spectral properties and finite-size effects, New Journal of Physics **22**, 085007 (2020).

[19] G. Passarelli, P. Lucignano, R. Fazio, and A. Russomanno, Dissipative time crystals with long-range Lindbladians, Phys. Rev. B **106**, 224308 (2022).

[20] F. Carollo and I. Lesanovsky, Exact solution of a boundary time-crystal phase transition: Time-translation symmetry breaking and non-markovian dynamics of correlations, Phys. Rev. A **105**, L040202 (2022).

[21] Y. Nakanishi and T. Sasamoto, Dissipative time crystals originating from parity-time symmetry, Phys. Rev. A **107**, L010201 (2023).

[22] D. Nemeth, A. Principi, and A. Nazir, Solving boundary time crystals via the superspin method (2025), arXiv:2507.06998 [quant-ph].

[23] F. Iemini, A. Russomanno, J. Keeling, M. Schirò, M. Dalmonte, and R. Fazio, Boundary Time Crystals, Phys. Rev. Lett. **121**, 035301 (2018).

[24] D. Nemeth, A. Nazir, R.-J. Slager, and A. Principi, (2026), The work underlying the operator space representation and classification is currently in preparation.

[25] J. Kruthoff, J. de Boer, J. van Wezel, C. L. Kane, and R. Slager, Topological Classification of Crystalline Insulators through Band Structure Combinatorics, Phys. Rev. X **7**, 041069 (2017).

[26] B. Bradlyn, L. Elcoro, J. Cano, M. G. Vergniory, Z. Wang, C. Felser, M. I. Aroyo, and B. A. Bernevig, Topological quantum chemistry, Nature **547**, 298 (2017).

[27] A. Bouhon, T. Bzdusek, and R. Slager, Geometric approach to fragile topology beyond symmetry indicators, Phys. Rev. B **102**, 115135 (2020).

[28] H. C. Po, A. Vishwanath, and H. Watanabe, Symmetry-based indicators of band topology in the 230 space groups, Nature Communications **8**, 50 (2017).

[29] P. W. Brouwer and V. Dwivedi, Homotopic classification of band structures: Stable, fragile, delicate, and stable representation-protected topology, Phys. Rev. B **108**, 155137 (2023).

[30] J. Provost and G. Vallee, Riemannian structure on manifolds of quantum states, Communications in Mathemat-

ical Physics **76**, 289 (1980).

[31] R. Resta, The insulating state of matter: a geometrical theory, The European Physical Journal B **79**, 121–137 (2011).

[32] P. Törmä, Essay: Where Can Quantum Geometry Lead Us?, Phys. Rev. Lett. **131**, 240001 (2023).

[33] A. Bouhon, A. Timmel, and R. Slager, Quantum geometry beyond projective single bands (2023), arXiv:2303.02180 [cond-mat.mes-hall].

[34] J. Ahn, G.-Y. Guo, and N. Nagaosa, Low-Frequency Divergence and Quantum Geometry of the Bulk Photovoltaic Effect in Topological Semimetals, Phys. Rev. X **10**, 041041 (2020).

[35] J. Yu, B. A. Bernevig, R. Queiroz, E. Rossi, P. Törmä, and B.-J. Yang, Quantum geometry in quantum materials, npj Quantum Materials **10**, 101 (2025).

[36] N. Hatano and D. R. Nelson, Localization Transitions in Non-Hermitian Quantum Mechanics, Phys. Rev. Lett. **77**, 570 (1996).

[37] C. M. Bender, Making sense of non-hermitian Hamiltonians, Reports on Progress in Physics **70**, 947 (2007).

[38] E. J. Bergholtz, J. C. Budich, and F. K. Kunst, Exceptional topology of non-Hermitian systems, Rev. Mod. Phys. **93**, 015005 (2021).

[39] H. Zhou and J. Y. Lee, Periodic table for topological bands with non-Hermitian symmetries, Phys. Rev. B **99**, 235112 (2019).

[40] K. Kawabata, K. Shiozaki, M. Ueda, and M. Sato, Symmetry and Topology in Non-Hermitian Physics, Phys. Rev. X **9**, 041015 (2019).

[41] D. S. Borgnia, A. J. Kruchkov, and R.-J. Slager, Non-Hermitian Boundary Modes and Topology, Phys. Rev. Lett. **124**, 056802 (2020).

[42] N. Okuma, K. Kawabata, K. Shiozaki, and M. Sato, Topological Origin of Non-Hermitian Skin Effects, Phys. Rev. Lett. **124**, 086801 (2020).

[43] T. Prosen, Third quantization: a general method to solve master equations for quadratic open Fermi systems, New Journal of Physics **10**, 043026 (2008).

[44] T. Prosen, Spectral theorem for the Lindblad equation for quadratic open fermionic systems, Journal of Statistical Mechanics: Theory and Experiment **2010**, P07020 (2010).

[45] S. Diehl, E. Rico, M. A. Baranov, and P. Zoller, Topology by dissipation in atomic quantum wires, Nature Physics **7**, 971 (2011).

[46] C.-E. Bardyn, M. A. Baranov, C. V. Kraus, E. Rico, A. İmamoğlu, P. Zoller, and S. Diehl, Topology by dissipation, New Journal of Physics **15**, 085001 (2013).

[47] S. Lieu, M. McGinley, and N. R. Cooper, Tenfold Way for Quadratic Lindbladians, Phys. Rev. Lett. **124**, 040401 (2020).

[48] F. Minganti, A. Miranowicz, R. W. Chhajlany, I. I. Arkhipov, and F. Nori, Hybrid-Liouvillian formalism connecting exceptional points of non-Hermitian Hamiltonians and Liouvillians via postselection of quantum trajectories, Phys. Rev. A **101**, 062112 (2020).

[49] Y. Michishita and R. Peters, Equivalence of Effective Non-Hermitian Hamiltonians in the Context of Open Quantum Systems and Strongly Correlated Electron Systems, Phys. Rev. Lett. **124**, 196401 (2020).

[50] C. C. Wanjura, M. Brunelli, and A. Nunnenkamp, Topological framework for directional amplification in driven-

dissipative cavity arrays, Nature Communications **11**, 3149 (2020).

[51] T. Haga, M. Nakagawa, R. Hamazaki, and M. Ueda, Liouvillian Skin Effect: Slowing Down of Relaxation Processes without Gap Closing, Phys. Rev. Lett. **127**, 070402 (2021).

[52] Z. Zhou and Z. Yu, Non-hermitian skin effect in quadratic Lindbladian systems: An adjoint fermion approach, Phys. Rev. A **106**, 032216 (2022).

[53] F. Yang, Q.-D. Jiang, and E. J. Bergholtz, Liouvillian skin effect in an exactly solvable model, Phys. Rev. Res. **4**, 023160 (2022).

[54] A. Chaduteau, D. K. K. Lee, and F. Schindler, Lindbladian versus Postselected non-Hermitian Topology, Phys. Rev. Lett. **136**, 016603 (2026).

[55] T. A. Loring, K-Theory and Pseudospectra for Topological Insulators, Annals of Physics **356**, 383–416 (2015).

[56] T. Loring and H. Schulz-Baldes, Finite volume calculation of K-theory invariants (2017), arXiv:1701.07455 [math-ph].

[57] A. Cerjan and T. A. Loring, Classifying photonic topology using the spectral localizer and numerical K-theory, APL Photonics **9**, 10.1063/5.0239018 (2024).

[58] K. Blum, Irreducible Components of the Density Matrix, in *Density Matrix Theory and Applications* (Springer Berlin Heidelberg, Berlin, Heidelberg, 2012) pp. 115–163.

[59] K. T. Hecht, Spherical Tensor Operators, in *Quantum Mechanics* (Springer New York, New York, NY, 2000) pp. 294–298.

[60] E. Fiorelli, M. Müller, I. Lesanovsky, and F. Carollo, Mean-field dynamics of open quantum systems with collective operator-valued rates: validity and application, New Journal of Physics **25**, 083010 (2023).

[61] A. Mukherjee, Y. Ibrahim, M. Hajdušek, and S. Vinjanampathy, Symmetries and correlations in continuous time crystals, Phys. Rev. A **110**, 012220 (2024).

[62] Z. Liu, Y. Li, Z. Fei, and X. Wang, Boundary Time Crystals: Beyond Mean-Field Theory (2025), arXiv:2510.03028 [quant-ph].

[63] Y. Huang, T. Wang, H. Yin, M. Jiang, Z. Luo, and X. Peng, Observation of continuous time crystals and quasi-crystals in spin gases, Nature Communications **16**, 9375 (2025).

[64] N. Lambert, E. Giguère, P. Menczel, B. Li, P. Hopf, G. Suárez, M. Gali, J. Lishman, R. Gadhvi, R. Agarwal, A. Galicia, N. Shammah, P. Nation, J. R. Johansson, S. Ahmed, S. Cross, A. Pitchford, and F. Nori, QuTiP 5: The Quantum Toolbox in Python (2024), arXiv:2412.04705 [quant-ph].

[65] N. Chadha, A. G. Moghaddam, J. van den Brink, and C. Fulga, Real-space topological localizer index to fully characterize the dislocation skin effect, Phys. Rev. B **109**, 035425 (2024).

[66] L. Jezequel, J. H. Bardarson, and A. G. Grushin, Explicit equivalence between the spectral localizer and local Chern and winding markers (2025), arXiv:2508.00214 [cond-mat.mes-hall].
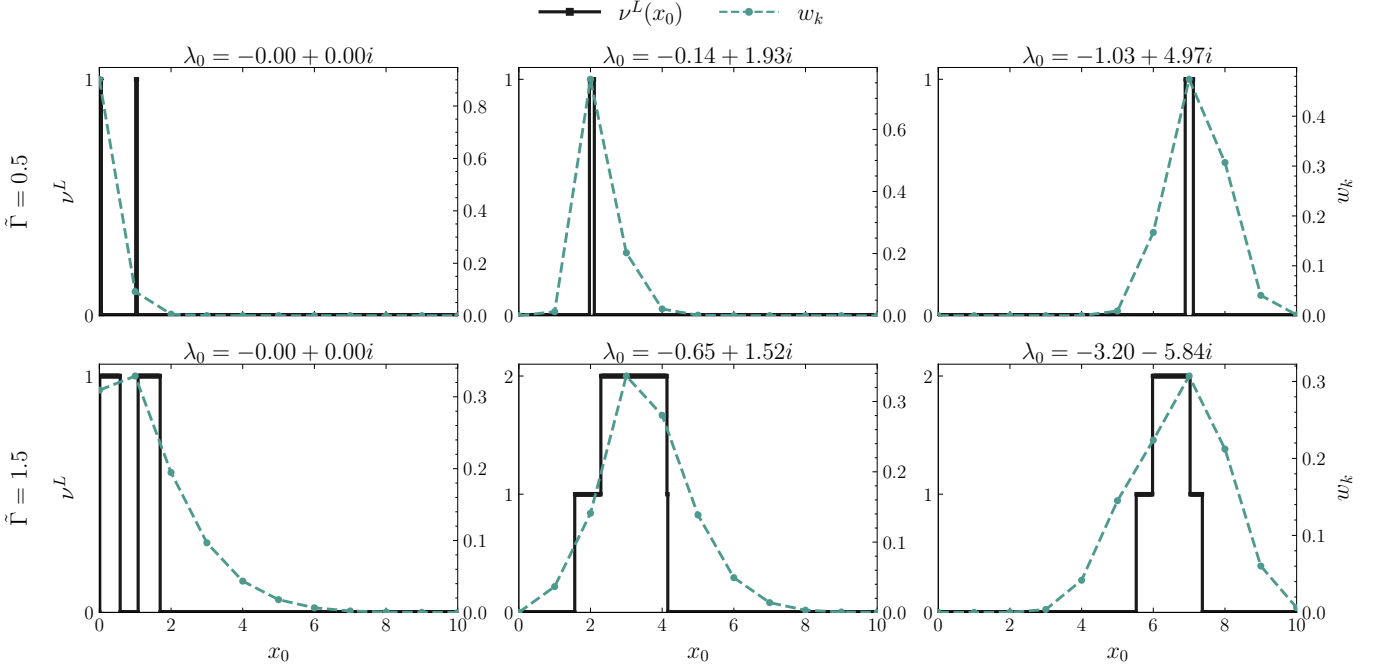
FIG. 4. Eigenmode Delocalization. Rank-resolved mode weights w_k are overlaid on the local topological domain structure $\nu^L(x_0)$. Six representative cases are shown, each labeled by the reference frequency λ_0 corresponding to a specific Liouvillian eigenmode. The first and second rows correspond to $\tilde{\Gamma} \equiv \Gamma/\Omega = 0.5$ and 1.5, respectively, with $N = 10$ throughout.

END MATTER

Details on Spectral Localizer—We prove that the definition of the spectral localizer in Eq. (4) is equivalent, up to a Pauli basis rotation, to the definition $L = (\tilde{X} + i\tilde{H})\Gamma$ as is typically used in non-Hermitian, one-dimensional chains [65]. Here, we set $\kappa = 1$, $\lambda_0 = 0$ and $x_0 = 0$ for ease of notation. The Hermitian Hamiltonian

$$\tilde{H} = \begin{pmatrix} 0 & \mathcal{L} \\ \mathcal{L}^\dagger & 0 \end{pmatrix}, \qquad (7)$$

is in class AIII, $\tilde{X} = \mathrm{diag}(\mathcal{X}, \mathcal{X})$ and $\Gamma = \mathrm{diag}(\mathbb{I}, -\mathbb{I})$ is a chiral matrix, such that $\tilde{H}$ exhibits the chiral symmetry $\Gamma\tilde{H} = -\tilde{H}\Gamma$. Using these definitions, one can show that

$$L = \begin{pmatrix} \mathcal{X} & -i\mathcal{L} \\ i\mathcal{L}^\dagger & -\mathcal{X} \end{pmatrix}, \qquad (8)$$

which by writing $\mathcal{L} = \mathrm{Re}(\mathcal{L}) + i\,\mathrm{Im}(\mathcal{L})$, where $\mathrm{Re}(\mathcal{L}) = \frac{1}{2}(\mathcal{L} + \mathcal{L}^\dagger)$ and $\mathrm{Im}(\mathcal{L}) = \frac{1}{2i}(\mathcal{L} - \mathcal{L}^\dagger)$ results in

$$L = \mathrm{Re}(\mathcal{L}) \otimes \sigma_y + \mathrm{Im}(\mathcal{L}) \otimes \sigma_x + \mathcal{X} \otimes \sigma_z. \qquad (9)$$

This is equivalent to Eq. (4) up to a rotation in of the Pauli basis $\sigma_{x,y,z}$. Therefore, the indices ν^L obtained through these are equal in magnitude and differ only in their sign. We employ our definition as in Eq. (4) to better motivate the notion of delocalization in complex frequency and the meaning behind the local Chern-type markers.

Note that this construction should not be confused with genuine Chern markers, which arise when the underlying base space is two-dimensional in physical or effective spatial coordinates. In the present case, the index is a point-gap invariant evaluated locally as a function of the complex spectral parameter λ_0. The resulting two-dimensional structure in the λ-plane reflects a complex frequency-resolved obstruction to simultaneous spectral and operator space localization, rather than a Chern curvature defined over a spatial manifold. The λ-plane plays the role of a parameter space over which ν^L is evaluated, producing isolated topological "islands" in spectral space.

Eigenmode Delocalization—We provide further numerical evidence for the eigenmode delocalization discussed above. To quantify the operator space structure of a Liouvillian eigenmode, we expand the right eigenvector corresponding to some chosen eigenvalue λ_0 of $\mathcal{L}$ in the spherical tensor basis, $|r^{(\alpha)}\rangle\rangle = \sum_{k,q} c_{kq}^{(\alpha)} |k\,q\rangle\rangle$, where the basis states $|k\,q\rangle\rangle$ are orthonormal under the Hilbert–Schmidt inner product and the normalization implies $\sum_{k,q} |c_{kq}^{(\alpha)}|^2 = 1$. The rank-resolved weights are then defined as $w_k^{(\alpha)} = \sum_q \left|c_{kq}^{(\alpha)}\right|^2$, which quantify how strongly the eigenmode occupies each irreducible rank-k sector. In Fig. 4, we overlay, for each Liouvillian eigenmode λ_0, the rank-resolved w_k with the corresponding local topological domain structure quantified by the spectral localizer index $\nu^L(x_0)$. As the rank coordinate x_0 is

scanned, eigenmodes are found to spread across the operator space chain precisely in regions where the local index is non-trivial. The onset and spatial extent of this spreading are aligned with the locations of the topological domains, indicating that these domains act as geometric sources of delocalization in operator space.

This behavior highlights that the relevant topology is inherently complex-frequency resolved. Rather than defining a single global topological phase, the localizer probes the obstruction structure associated with a fixed spectral point λ_0. As a result, different eigenmodes experience distinct patterns of topological domains along the operator space chain: domains may appear at different locations for different λ_0, and with increasing dissipation they can expand and merge without necessarily spanning the entire chain. Operator space delocalization is therefore mode-dependent, with each eigenmode exhibiting a characteristic spatial profile across tensor-rank sectors.

SUPPLEMENTARY MATERIAL: SPECTRAL LOCALIZER

In the Supplementary Material, we provide additional details on the implementation of the spectral localizer, with particular emphasis on the choice of the parameter κ (see Eq. (4) of the main text).

In Ref. [66] it was shown that, in one dimension, the point-gap winding marker arises as the leading non-vanishing term in a controlled small-κ expansion of the spectral localizer index. In practice, there exists a finite κ-interval, a stability window, within which the index faithfully captures the underlying point-gap topology [57]. Throughout this work, we fix $\kappa = 1$, chosen within the numerically verified κ-stable regime, where the localizer gap remains open and the topological classification is stable under variations in κ. In this regime, the index faithfully captures the intrinsic point-gap topology while resolving its spatial structure. The parameter κ controls the relative weighting between spectral and positional contributions in the localizer, with κ^{-1} setting the effective spatial resolution scale over which the topology is probed [57].

In Figs. S1 and S2 we demonstrate that the non-trivial topology remains stable over a broad window of κ. For small κ, the localizer probes the system over an effectively large spatial scale, rendering it insensitive to fine, spatially resolved structure. As a result, smaller topological domains are smeared out. In the intermediate regime $\kappa \in [0.5, 2]$, the localizer achieves optimal resolution, clearly resolving localized topological domains. For larger κ, however, the probe becomes overly localized and begins to over-resolve short-scale changes.

We further examine the behavior of the localizer gap $\mu_{(x_0, \lambda_0)}$ as a function of x_0. Within topologically non-trivial regions the gap remains open, while it exhibits sharp dips at the boundaries between domains, signaling local topological transitions.

In addition, we probe the robustness of the topology by sweeping λ_0 at fixed position x_0, as shown in Fig. S3. We focus on the slowest-decaying oscillatory modes, corresponding to eigenvalues with the least negative $\text{Re}(\lambda)$, and fix $x_0 = 1$. The topological islands are most clearly resolved within the intermediate window $\kappa \in [0.5, 2]$, where the localizer gap μ remains open throughout these regions.
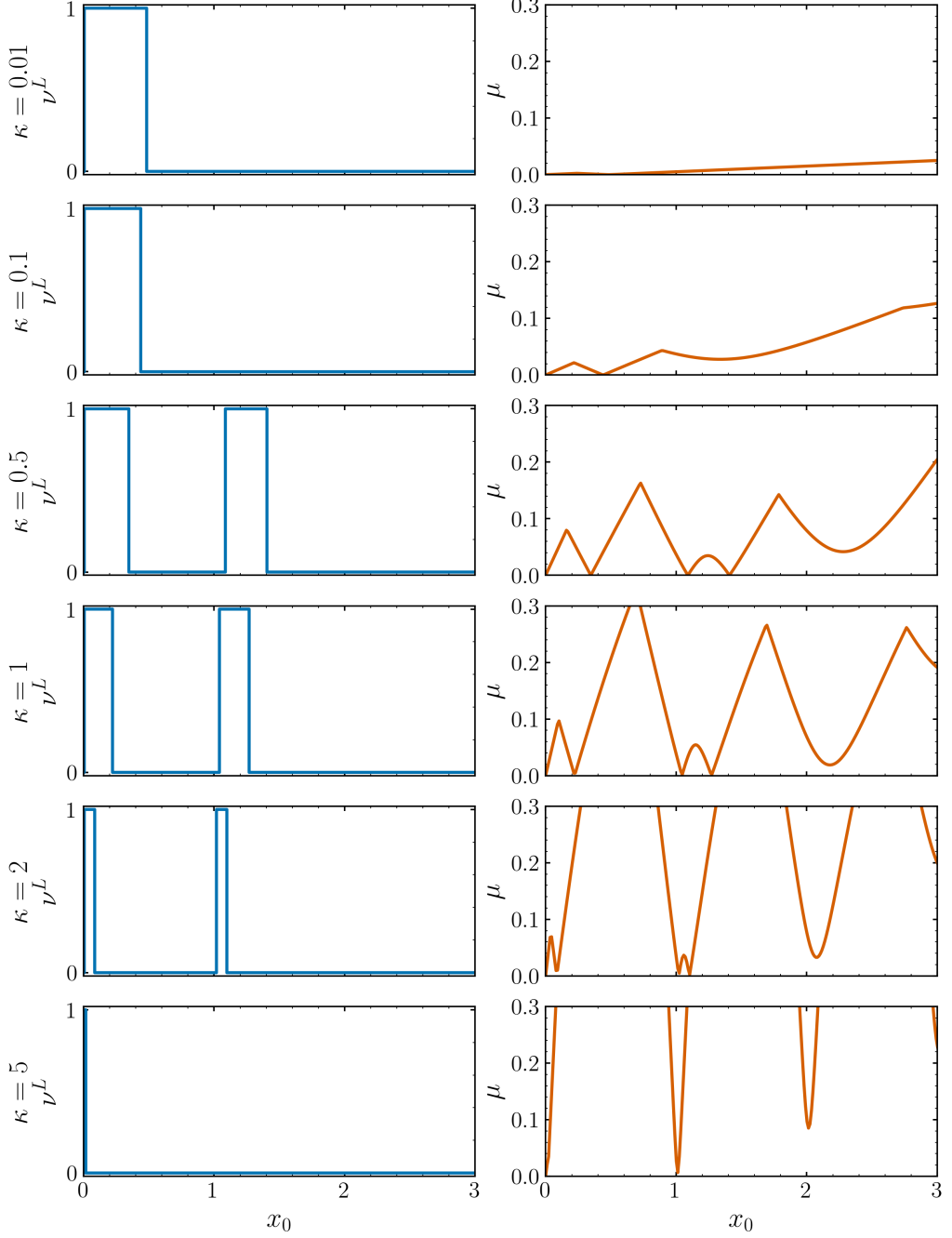
FIG. S1. Topological Domains as a Function of κ. We show the dependence of the localizer index ν^L and gap μ on the resolution parameter κ for $\kappa \in \{0.01, 0.1, 0.5, 1, 2, 5\}$ and fixed $\lambda_0 = 0$. A stable κ-window is observed in which the gap remains open (inside topologically non-trivial regions) and the topological classification is unchanged. Results are shown for fixed $\tilde{\Gamma} \equiv \Gamma/\Omega = 1$, system size $N = 10$ and are truncated to $x_0 \leq 3$ (beyond which ν^L remains zero.).
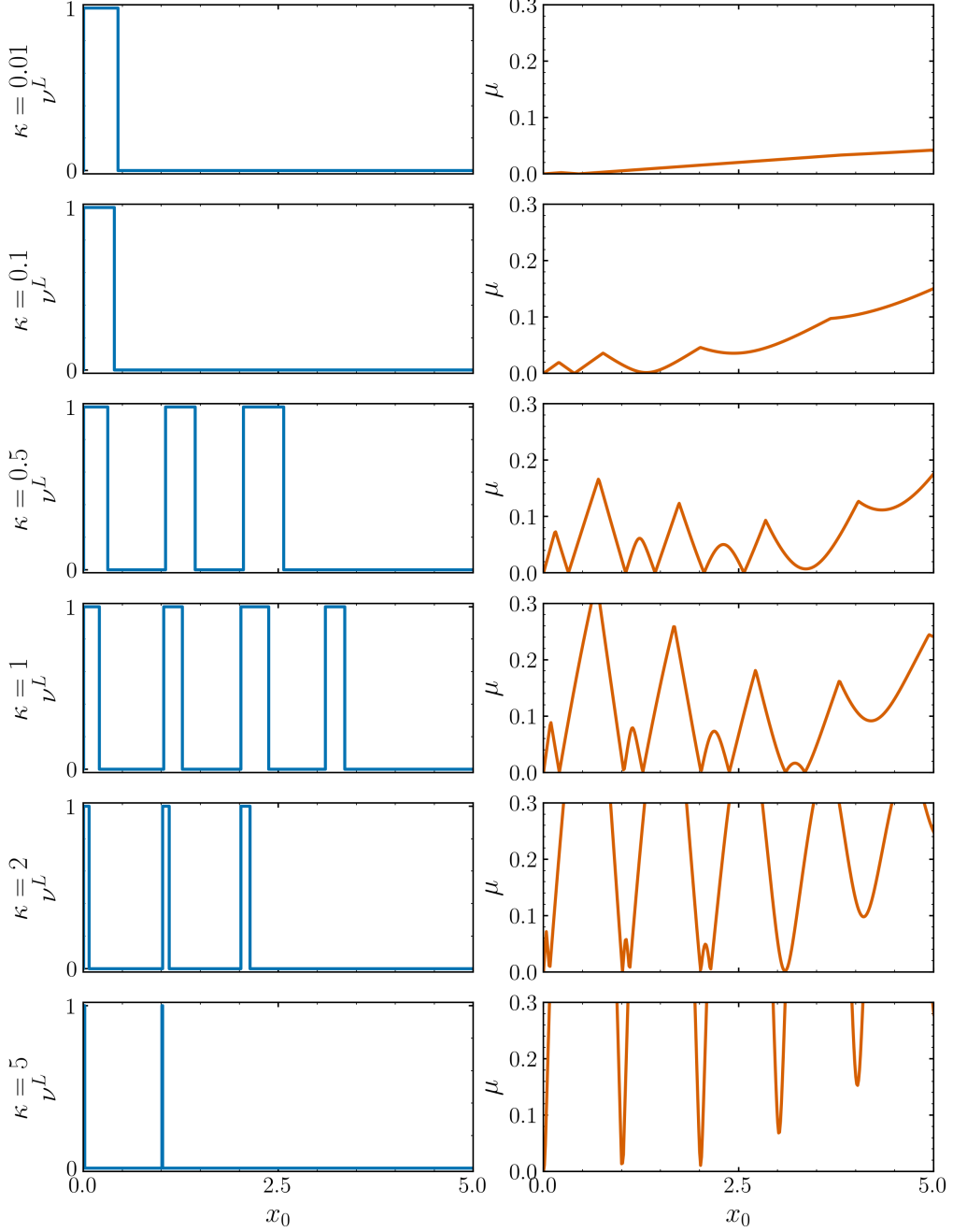
FIG. S2. Topological Domains as a Function of κ. We show the dependence of the localizer index ν^L and gap μ on the resolution parameter κ for $\kappa \in \{0.01, 0.1, 0.5, 1, 2, 5\}$ and fixed $\lambda_0 = 0$. A stable κ-window is observed in which the gap remains open (inside topologically non-trivial regions) and the topological classification is unchanged. Results are shown for fixed $\tilde{\Gamma} \equiv \Gamma/\Omega = 1$, system size $N = 20$ and are truncated to $x_0 \leq 5$ (beyond which ν^L remains zero.).
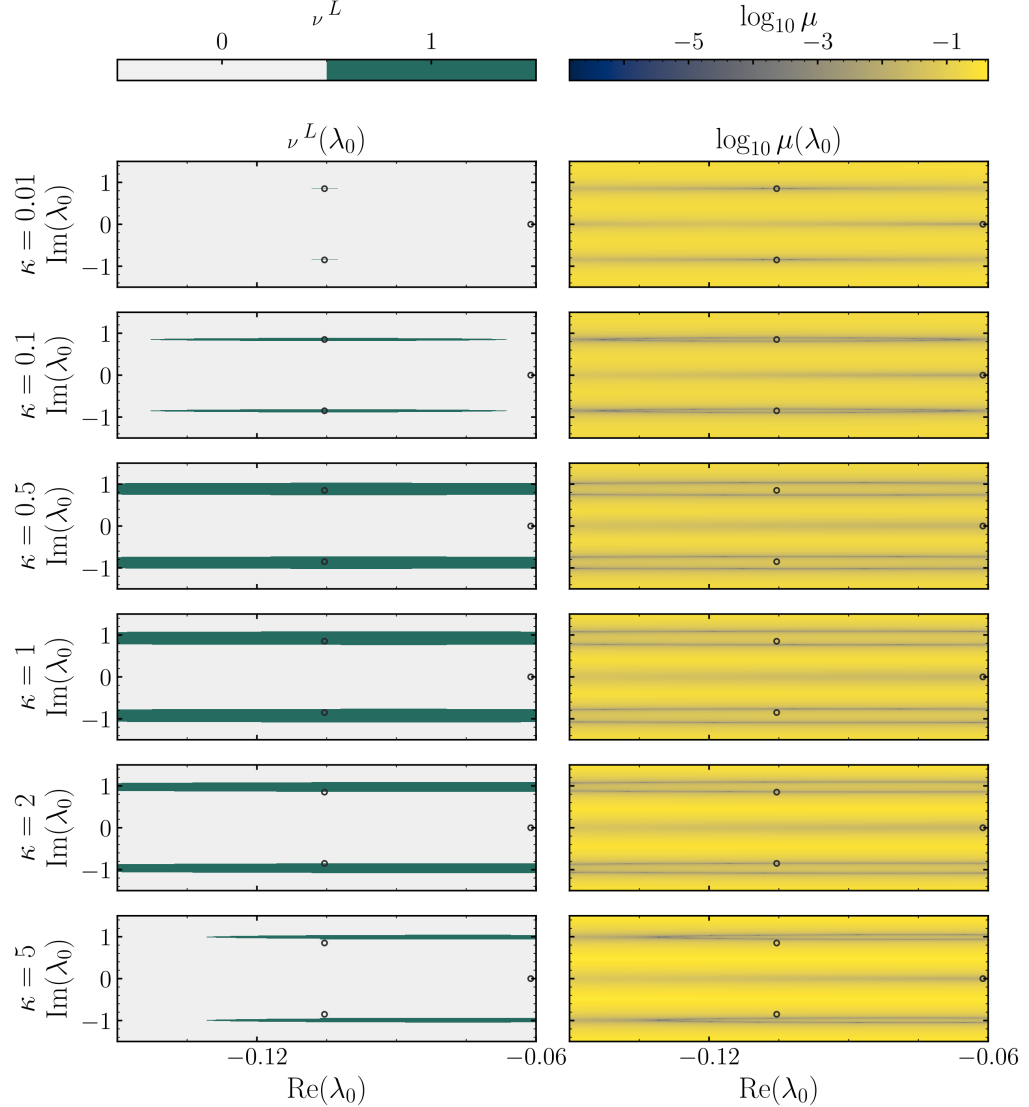
FIG. S3. Spectral Islands as a Function of κ. We show the dependence of the localizer index ν^L and gap μ on the resolution parameter κ for $\kappa \in \{0.01, 0.1, 0.5, 1, 2, 5\}$ and fixed $x_0 = 1$. Hollow circular markers denote the eigenvalues of the Liouvillian $\mathcal{L}$. A stable κ-window is observed in which the gap remains open (inside topologically non-trivial regions) and the topological classification is unchanged. Results are shown for fixed $\tilde{\Gamma} \equiv \Gamma/\Omega = 1$ and system size $N = 10$. Here, we focus on the slowest-decaying oscillatory pair of eigenmodes.